remote sensing

MDPI

Article

Evaluation of SNPP and NOAA-20 VIIRS Datasets Using RadCalNet and Landsat 8/OLI Data

Xin Jing *, Sirish Uprety, Tung-Chang Liu, Bin Zhang and Xi Shao

Cooperative Institute for Satellite Earth System Studies (CISESS), Earth System Science Interdisciplinary Research Center, University of Maryland, College Park, MD 20740, USA
* Correspondence: xinjing@umd.edu

Abstract: In this study, we used RVUS data from RadCalNet as a benchmark to verify the radiometric accuracy and stability of operational and reprocessed SNPP/VIIRS data and the accuracy of NOAA-20/VIIRS data, as well as to assess the efficiency of the SNPP/VIIRS reprocessing algorithm. In addition, to remove the uncertainty of the RVUS site itself, we used Landsat 8/OLI as another benchmark with which to validate the accuracy and stability of VIIRS data through the RUVS site. The radiometric biases of the operational and reprocessed SNPP VIIRS bands were within ±4% and ±2%, respectively, as compared with the RUVS site and OLI, except for the M10 and M11 bands. In particular, the biases of the M5 and M7 bands were reduced by ~2% in this study. NOAA-20 VIIRS, on the other hand, was consistently lower than SNPP by ~2 to ~4% for all the bands. For the equivalent bands, the drift differences between operational and reprocessed SNPP/VIIRS and OLI were no larger than 0.24%/year and 0.1%/year, respectively. The reprocessing algorithm of SNPP VIIRS efficiently improved the radiometric accuracy and stability of the SNPP/VIIRS dataset to meet its specifications.

Keywords: RadCalNet; evaluation; SNPP; NOAA-20; VIIRS; Landsat 8

Citation: Jing, X.; Uprety, S.; Liu, T.-C.; Zhang, B.; Shao, X. Evaluation of SNPP and NOAA-20 VIIRS Datasets Using RadCalNet and Landsat 8/OLI Data. *Remote Sens.* **2022**, *14*, 3913. https://doi.org/10.3390/rs14163913

Academic Editor: Jie Cheng

Received: 13 June 2022
Accepted: 10 August 2022
Published: 12 August 2022

1. Introduction

Suomi National Polar-orbiting Partnership (SNPP) and NOAA-20 have been operating successfully since their respective launches on 28 October 2011 and 18 November 2017. The Visible Infrared Imaging Radiometer Suite (VIIRS), which is one of the key instruments onboard the SNPP and NOAA-20, provides data for a large number of applications, including weather and climate, imagery of the Earth, land-use/land-cover change, urban and regional development, vegetation health for agriculture and food production, albedo, aerosols and air quality, and the monitoring of endangered species. For many quantitative applications, imaging radiometers need to be calibrated and data products need to be continuously validated on orbit. During the early days of SNPP/VIIRS operational calibration and data production, there were inconsistencies in both the algorithms and calibration inputs for several reasons [1]. To address the issues, the National Oceanic and Atmospheric Administration (NOAA)/National Environmental Satellite, Data, and Information Service (NESDIS)/Center for Satellite Applications and Research developed a comprehensive algorithm, and recalibrated and reprocessed the SNPP/VIIRS operational radiometric data. It is important to evaluate the radiometric accuracy and stability of the reprocessed SNPP/VIIRS dataset. In addition, the Committee on Earth Observation Satellites Working Group on Calibration and Validation (CEOS-WGCV) established a working group to coordinate the development of the Radiometric Calibration Network (RadCalNet) for performing automated radiometric calibration using member-provided resources. This provides automated in situ measurements and estimates of propagated top-of-atmosphere (TOA) reflectance. RadCalNet has been shown to be a useful and SI-traceable radiometric calibration method [2].

In this study, we used one of the RadCalNet sites—the Railroad Valley Playa in the US (RVUS)—to evaluate the radiometric accuracy and stability of the operational and reprocessed SNPP/VIIRS to verify the effectiveness of the reprocessing algorithm and the radiometric accuracy of the NOAA-20/VIIRS. Furthermore, as the possible degradation of the RVUS site itself was observed in the data analysis, another benchmark that has proven to be highly accurate and stable—Landsat 8 Operational Land Imager (OLI) data—was used to perform a relative comparison with the VIIRS dataset to confirm their radiometric accuracy and stability. The paper is organized as follows. In Section 2, the RadCalNet RVUS site and the sensor data analyzed in this paper are introduced. Section 3 describes the data processing steps and methodologies used to conduct the study. In Section 4, the radiometric performance of the VIIRS datasets is evaluated through a comparison with the RVUS site and Landsat 8/OLI. Conclusions are summarized in Section 5.

2. RadCalNet Site and Sensor Overview

2.1. RadCalNet RVUS Site Overview

RadCalNet currently contains four sites, including the Railroad Valley Playa in the US (RVUS), the LaCrau site in France (LCFR), the Gobabeb (GONA) site in Namibia, the Baotou site in China (BTCN), and the Baotou sandy site in China (BSCN) [3]. These sites use automated in situ systems to increase the number of sensor overpass dates with corresponding ground truth data. The automated measurements include surface reflectance and atmospheric measurements acquired every 30 min between 09:00 and 15:00 local time. Nadir-viewing instruments with a 10 nm spectral resolution acquire the surface reflectance measurements at wavelengths between 400 and 2500 nm. Surface pressure, columnar water vapor, columnar ozone, aerosol optical depth at 550 nm, and Angstrom coefficient measurements serve as inputs to a Radiative Transfer Model (RTM) that predicts the corresponding nadir-view TOA reflectance. The RadCalNet data are available through the RadCalNet portal [4]. The surface types of the four sites are dry lake bed, sparse vegetation covered with pebble soil, sand and gravel with some widely scattered dry grass, and artificial targets for RVUS, LCFR, GONA, and BTCN, respectively. Moreover, the start dates of the data on these four sites are May 2013, January 2015, July 2017, and April 2016, respectively. Considering the data availability, the geometric size of the RadCalNet sites, and their surface type, and in order to avoid edge effects given the spatial resolution of bands of interest of the VIIRS (750 m) studied in this work, only the RVUS site was used.

RVUS is located in Nevada and is currently maintained and operated by the Remote Sensing Group (RSG) at the University of Arizona (UoA). It also hosts an earlier RSG-developed automated network known as the Radiometric Calibration Test Site (RadCaTS) [5]. The instruments used to determine the surface reflectance are multispectral ground-viewing radiometers (GVRs), which were developed by the Remote Sensing Group at the UoA [6]. The current suite of RadCaTS instruments includes four GVRs in a nadir-viewing configuration [7], scattered over a 1 km $\times$ 1 km area centered at latitude 38.497°N and longitude 115.690°W [6,8], as shown by the red square in Figure 1; the TOA reflectance spectra are representative of this square region. In addition, RVUS consists of compacted clay-rich lake deposits, which is a spatially uniform section of dry lake bed that forms a relatively smooth surface, as can be seen from Figure 1. In addition, RVUS provides data including early RadCaTS, with a start date of May 2013. Therefore, considering its 9-year data time period, its adequate site reflectivity observation coverage, and the homogeneity of the site, RVUS is ideal for long-time low-resolution satellite sensor calibrations.

2.2. Sensor Overview

2.2.1. Landsat 8/OLI

In the data analysis, we found a slight degradation of the RVUS site itself (which is illustrated in Section 3.6). In order to minimize its influence on the validation results, we also used Landsat 8 Operational Land Imager (OLI) as another benchmark to evaluate the radiometric performance and on-orbit stability of the VIIRS sensors.

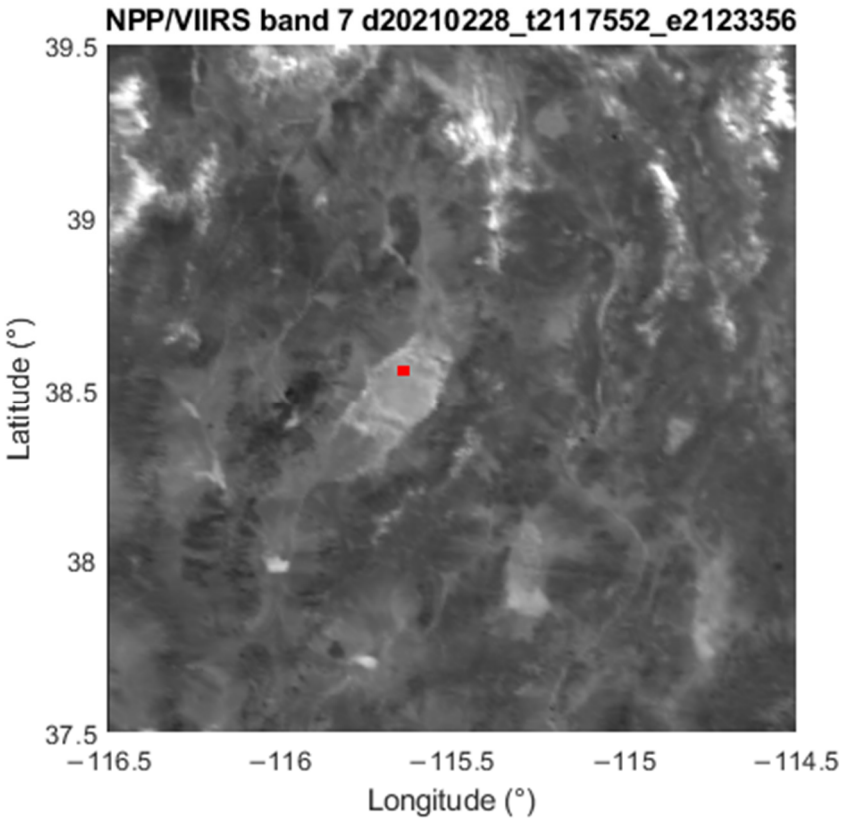

Figure 1. 28 February 2021 SNPP/VIIRS band 7 image in RVUS. The red square indicates the effective range of ground-based spectral measurements.

Landsat 8 was launched on 11 February 2013. The satellite collects images of the Earth with a 16-day repeat cycle, referenced to the Worldwide Reference System-2. The approximate scene size is 170 km north–south by 183 m east–west. The satellite carries the Operational Land Imager and the Thermal Infrared Sensor (TIRS) instruments. OLI is a visible and near-infrared (VNIR) multispectral sensor that operates in the range 400–2500 nm, and TIRS is a two-band thermal sensor that operates in the range 10.6–12.5 µm [9]. This work focuses on the radiometric performance of VNIR bands, and only OLI was used as the reference. OLI measures in the visible, near-infrared, and short-wave infrared portions of the spectrum. The data files consist of 11 spectral bands with a spatial resolution of 30 m for bands 1–7 and bands 9–11, and 15 m for the panchromatic band 8. Table 1 shows the wavelength and resolution of the OLI bands used in this work.

Table 1. Wavelengths and resolutions of the bands of VIIRS and OLI sensors.

	NPP and NOAA-20/VIIRS			**Landsat 8/OLI**	
Launch	**28 October 2011 and 18 November 2017**			**11 February 2013**	
	Wavelength (um)	**Spatial Resolution (m)**		**Wavelength (um)**	**Spatial Resolution (m)**
M1	0.402–0.422	750			
M2	0.436–0.454	750	B1	0.43–0.45	30
M3	0.478–0.488	750	B2	0.45–0.51	30
M4	0.545–0.565	750	B3	0.53–0.59	30
M5	0.662–0.682	750	B4	0.64–0.67	30
M7	0.846–0.885	750	B5	0.85–0.88	30
M8	1.23–1.25	750			
M10	1.58–1.64	750	B6	1.57–1.65	30
M11	2.23–2.28	750	B7	2.11–2.29	30

According to previous research, OLI has been shown to be radiometrically stable to better than 0.1% [10]. The coastal/aerosol (CA) band (B1) has exhibited degradation in radiometric sensitivity over its lifetime [11], and this degradation has been tracked and was corrected in a reprocessing effort in February–May 2017 [12,13]. The other OLI bands were corrected for a small change in sensitivity in September–October 2013, but since then, they have all remained stable [11]. Validation of the absolute radiometric calibration of OLI has shown the instrument to be within ±2% in terms of reflectance [14,15]. As a result of the high-precision radiometric performance of Landsat 8 and its stability, we used Landsat 8 as another benchmark to evaluate the radiometric performance of VIIRS sensors and the stability of SNPP/VIIRS in this study.

To convert the digital value of OLI to TOA reflectance, the following equation was used:

$$\rho_\lambda = \frac{(M_\rho \times DN + A_\rho) \times d^2}{\cos(\theta_{SZA})} \quad (1)$$

where M_ρ is a band-specific multiplicative rescaling factor, A_ρ is a band-specific additive rescaling factor, d is Earth–Sun distance in astronomical units, θ_{SZA} is the solar zenith angle for each pixel in the processed ROI, DN is the (calibrated) pixel digital values, and ρ_λ is the final TOA reflectance. A metadata file included with the OLI image data products provides specific values for the rescaling factors [16].

2.2.2. SNPP and NOAA-20/VIIRS

The SNPP satellite was launched on 28 October 2011. NOAA-20, the second spacecraft in NOAA's next-generation polar orbiting satellites, was launched on 18 November 2017. Both SNPP and NOAA-20 carry the VIIRS, a 22-band visible/infrared sensor. SNPP crosses the equator at about 01:30 and 13:30 local time, providing twice-daily coverage of the entire earth. The transit times of SNPP and NOAA-20 VIIRS differ by about 50 min. The 11 VNIR moderate resolution channels of SNPP and NOAA-20 VIIRS cover a spectral range from 410 nm to 2257 nm, with a spatial resolution of 750 m. The moderate-resolution bands have 3200 pixels across a scan within a scan angle of ±56.28° from the nadir [17–22]. Since SNPP and NOAA-20 use different solar irradiance models, this study only verified their reflectance performance and did not discuss irradiance [23].

Since VIIRS M7 and M9 are ocean color aerosol and cirrus cloud cover bands, the radiometric performance of the SNPP Sensor Data Record (SDR) for the M1, M2, M3, M4, M5, M7, M8, M10, and M11 bands was evaluated and the radiometric consistency between the SNPP and NOAA-20 was compared on the RVUS site in this work. In addition, the OLI B1 to B7 bands were used as a benchmark to evaluate the radiometric consistency with the VIIRS spectral equivalent bands, i.e., the VIIRS M2, M3, M4, M5, M7, M10, and M11 bands. Table 1 shows the wavelength and resolution of the VIIRS bands used in this work. Figure 2 shows their relative spectral response functions, and it can be seen that the OLI wavelength is wider than that of VIIRS for the majority of equivalent bands.

During the early days of SNPP/VIIRS operational calibration and data production, there were inconsistencies in both the algorithms and calibration inputs for several reasons. More details to this end can be found in [1]. As revealed in previous studies, one of the major issues related to absolute accuracy is that, based on comparisons with MODIS and independent observations, there are radiometric biases in the M5 and M7 bands, i.e., they are about 2% higher than what they should be [1]. As for the long-term radiometric stability of SNPP/VIIRS, its requirement of 0.3%/year is far more stringent than the absolute calibration accuracy (±2%). To address these issues, the NOAA/NESDIS/Center for Satellite Applications and Research developed a comprehensive algorithm, and recalibrated and reprocessed the SNPP/VIIRS radiometric operational data produced since the launch. In the recalibration, they resolved inconsistencies in the processing algorithms, terrain correction, straylight correction, and anomalies in the thermal bands. To improve the accuracy and stability of the reflective solar bands, they developed a comprehensive approach, i.e., the Kalman filtering model, to incorporate onboard solar, lunar, desert site, intersatellite

calibration, and a deep convective cloud calibration methodology. They further developed and implemented the Solar Diffuser Surface Roughness Rayleigh Scattering model to account for sensor responsivity degradation in the near-infrared bands. Considering so many improvements, it is extremely important to evaluate the radiometric accuracy and stability of the data. The reprocessed SNPP/VIIRS data were evaluated in this study in order to validate the efficiency of the recalibration algorithms. The reprocessed data are now available from 2012 to 2020 on request and will eventually be archived in the NOAA Comprehensive Large Array-data Stewardship System (CLASS) database [1,24].

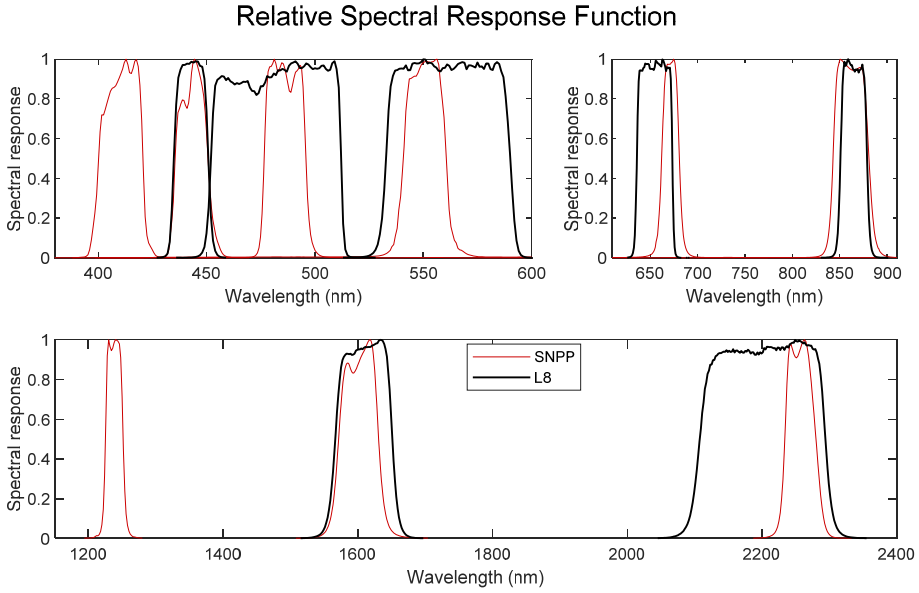

Figure 2. Relative spectral response functions of Landsat 8/OLI, SNPP/VIIRS.

3. Methodology

Each sensor's imaging timetable was checked against the date of the RadCalNet data acquisition. When a sensor of interest imaged the site and RadCalNet acquired the corresponding surface measurements, the dates were selected as overpass dates. The selected image datasets were downloaded from the sensor operator. Landsat 8/OLI, operational SNPP, and NOAA-20 VIIRS image data were downloaded through the US Geological Survey (USGS) EarthExplorer portal and the NOAA CLASS electronic library, respectively, and reprocessed SNPP/VIIRS image data were requested and downloaded from NOAA/NESDIS. All downloaded image data products were preprocessed by the sensor operator's ground processing system with full radiometric correction and precision geometric registration/correction. The data preprocessing steps in this paper mainly refer to the work from [2] but were specifically modified for VIIRS sensors as follows.

3.1. Image ROI Reflectance Extraction

Given the spatial resolution of the sensors and the representative region of the RadCalNet RVUS TOA reflectances, 1 km $\times$ 1 km regions of interest (ROI) were selected; these were centered at the representative region's latitude/longitude coordinates given in Section 2.1. We then extracted the ROI from satellites images by averaging the physical quantities whose pixel coordinates were in the range of 1 km $\times$ 1 km.

3.2. RadCalNet RVUS Reflectance Extraction

In order to obtain the RadCalNet reflectance for OLI and VIIRS equivalent bands, first, the TOA reflectance data from the RadCalNet RVUS site for collocation dates were extracted. Second, the extracted spectra were linearly interpolated to estimate the TOA reflectance at the sensor overpass times. Third, the relative spectral response of the sensors was interpolated to 10 nm to match the spectral resolution of the RadCalNet spectral

data. Lastly, the RadCalNet spectral measurements were normalized to the corresponding multispectral value for the sensor of interest in order to allow for a direct comparison with the sensor-measured TOA reflectance:

$$\rho_{\mathrm{RCN}} = \frac{\int \rho_{\mathrm{H}} RSR \, d\lambda}{\int RSR \, d\lambda} \tag{2}$$

where ρ^{H} is the RadCalNet TOA spectral reflectance, RSR is the relative spectral response function of the sensors, λ is the wavelength, and ρ_{RCN} is the integrated equivalent reflectance of the RadCalNet-predicted TOA reflectance in the specific sensor band.

3.3. Cloud and Cloud Shadow Filtering

RadCalNet collects data in clear sky conditions only and the fill value is used in the input file when it does not meet the QA requirements for release. This may include scenarios in which no data are available for an unspecified reason, TOA reflectance is not processed, or there are anomalous atmospheric or surface conditions [25]. In order to ensure the data are as clean as possible, we selected collocation only when the input data of RadCalNet had no fill value within half an hour before and after the satellite transit time. Moreover, we found that there were still outliers even after using the aforementioned filtering characteristics, so we used ECMWF's Total Cloud Cover (TCC) data product to further remove the possible cloudy days, and the threshold value of TCC was set to 0.2. Table 2 shows the number of data points before and after using TCC filtering. It can be seen that for SNPP and NOAA-20 VIIRS images, approximately 10% of the data points were removed after TCC filtering. For Landsat 8, there was no change because the land cloud cover criteria were applied when downloading the images. Note that the start date of NOAA-20 from CLASS was 1 February 2018 though its launch date was 18 November 2017.

Table 2. The number of data points for each preprocessing step.

	Number of Data Points		
	L8	**SNPP**	**N20**
Time period	1 May 2013 to 1 September 2019		1 February 2018 to 1 September 2019
collocation	44	1042	251
TCC	44	949	227
VZA	44	150	28

3.4. Image View Zenith Angle Selection

Figure 3 shows the radial plot of the solar and viewing geometry over the RVUS for Landsat 8/OLI, S-NPP/VIIRS, and NOAA-20/VIIRS, respectively. The viewing zenith angle (VZA) with reference to the ROI of Landsat 8/OLI varied in a range of 1°, observing the target from the nadir; the viewing angle effects could be considered insignificant. The SNPP and NOAA-20, on the other hand, had variable viewing angles from −57° to 57° and observed the target ROI from both east and west directions; thus, the viewing angle effect needed to be considered.

In order to reduce the impact of the viewing angle on the validation results, simple preprocessing steps were needed. First, we removed data points in which the viewing angles were too large and only the SNPP and NOAA-20 images with VZA within ±13° were used to perform the evaluation. It can be seen from Table 2 that only 16% and 13% of the data points remained after limiting the VZA for SNPP and NOAA-20, respectively. Thereafter, a simple viewing angle effects correction method used in previous work was applied to correct the viewing angle effect [25–27]. This method proved to be effective in reducing the uncertainty of the radiance difference between RVUS and sensor measurements due to the viewing angle effect.

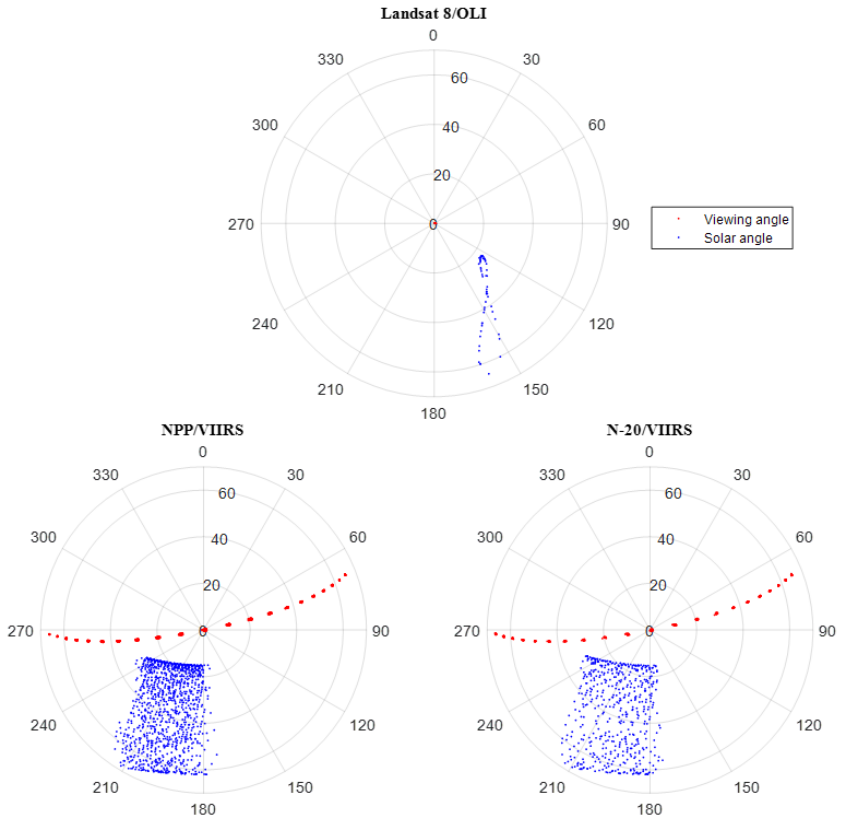

Figure 3. Solar (blue) and viewing (red) angular distribution of Landsat 8/OLI, SNPP/VIIRS, and NOAA-20/VIIRS, and the time periods are 22 May 2013 to 12 May 2021, 2 April 2013 to 20 July 2021, and 13 February 2018 to 20 July 2021, respectively. The angular direction (degrees east of north) in polar coordinates indicates the azimuth angle and the length of the radius specifies the zenith angle.

First, linear regression was performed on the observed TOA reflectances versus the variable $\sin\theta_z \sin\theta_a$ to obtain the correction coefficients a and b:

$$\rho_i^{\mathrm{VIIRS}} = a \times \sin\theta_z \sin\theta_a + b, \tag{3}$$

where ρ_i^{VIIRS} is the VIIRS TOA reflectance measured on date i, θ_z and θ_a are the sensor viewing zenith and viewing azimuth angles, respectively. A 'base' TOA reflectance ρ^r was then estimated from the mean reflectance across all dates. Finally, the corrected reflectance ρ_i^c was calculated as the ratio of the observed and regression-predicted TOA reflectances scaled by the 'base' reflectance:

$$\rho_i^c = \frac{\rho^r \times \rho_i^{\mathrm{VIIRS}}}{a \times \sin\theta_z \sin\theta_a + b}. \tag{4}$$

3.5. Radiometric Performance and Stability Analysis

In this study, the percentage of TOA reflectance ratio (bias) and the ratio drift were used as indices to evaluate the radiometric performance and stability, respectively, of the VIIRS datasets. The reflectance ratio percentage was calculated as follows:

$$R\% = \left(\frac{\rho_S^c}{\rho_{\mathrm{RCN}}} - 1\right) \times 100 \tag{5}$$

where ρ_S^c is the viewing angle effect corrected sensor-measured TOA reflectance, ρ_{RCN} is the corresponding RadCalNet-predicted TOA reflectance, and $R\%$ is the reflectance ratio percentage in TOA reflectance.

From the aforementioned processing procedure, a time series of TOA reflectance ratio data points was generated for the RadCalNet RVUS site. To evaluate the long-term potential drift in each sensor band, linear regressions of the reflectance ratio versus days were fitted to the TOA reflectance ratio. The regression slope α was normalized by the intercept β to derive a percent yearly drift $d\%/year$:

$$d\%/year = \frac{\alpha \times 365 \times 100}{\beta}. \quad (6)$$

3.6. Time Selection of Data for Analysis

During the analysis, the unexpected radiometric degradation over RVUS was noticed. Since SNPP/VIIRS only reprocessed data available until 2020, in order to illustrate the degradation phenomenon of RVUS, operational SNPP/VIIRS data released on the NOAA CLASS website were used. Figure 4 shows the time series of reflectance ratios between Landsat-8/OLI, SNPP/VIIRS, NOAA-20/VIIRS, and RadCalNet over RVUS. The time series ratios of the three sensors and the yearly drift of OLI and operational SNPP/VIIRS were consistent, indicating that the significant drift was likely due to the RVUS site not the sensors. We do not know the reasons for the radiometric degradation of the RVUS site; therefore, only time periods that did not exhibit a significant decrease, i.e., May 2013 to August 2019, were selected to analyze the radiometric characteristics of the VIIRS sensors.

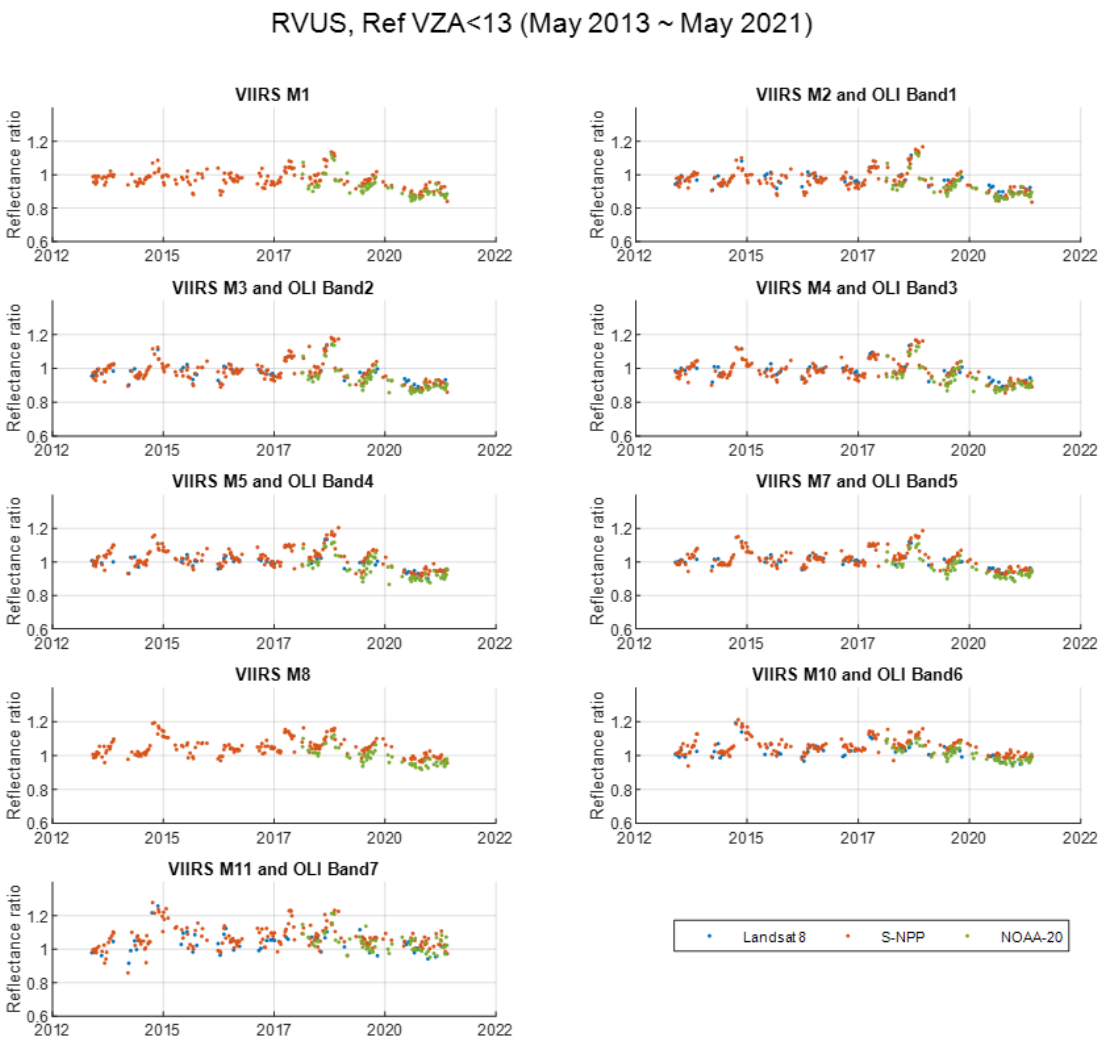

Figure 4. The time series of the reflectance ratio between RadCalNet with Landsat-8/OLI, operational SNPP/VIIRS, and NOAA-20/VIIRS over RVUS from May 2013 to May 2021.

4. Results

4.1. SNPP Operational and Reprocessed Data Comparison Results

4.1.1. Comparison Results of the Reflectance Ratio Percentage

Figure 5 shows the average reflectance ratio percentage, i.e., the bias, between Landsat 8/OLI, operational and reprocessed SNPP/VIIRS, and RadCalNet at RVUS from May 2013 to August 2019. Table 3 lists the results. It can be seen from Figure 5 that, as compared to RVUS, the average reflectance ratio percentages of operational and reprocessed SNPP/VIIRS were all within 5%, except the VIIRS M8, M10, and M11 bands. In particular, the biases between the reprocessed SNPP/VIIRS and RVUS site were all within 2%, except the M8, M10, and M11 bands, which meets the VIIRS radiometric performance specifications and is consistent with previous work [7]. Moreover, the larger bias of the M8, M10, and M11 bands may be due to the lower solar radiation signal. In addition, similar results concerning the inconsistency between OLI B7 and operational VIIRS M11 were noted in previous work [28]. The biases between OLI and RVUS were within ±4% across all bands. In particular, the longer wavelength B6 and B7 bands exhibited a larger relative bias, i.e., 2.86% and 3.97%, respectively. The comparison results of OLI over RVUS were consistent with those reported in previous work [2]. With respect to the standard deviation, the VIIRS (~4.5% to ~7.7%) bands were larger than OLI (~3.5% to ~6%), most likely due to the impact of the residual solar and viewing angle and the wider wavelength width of OLI.

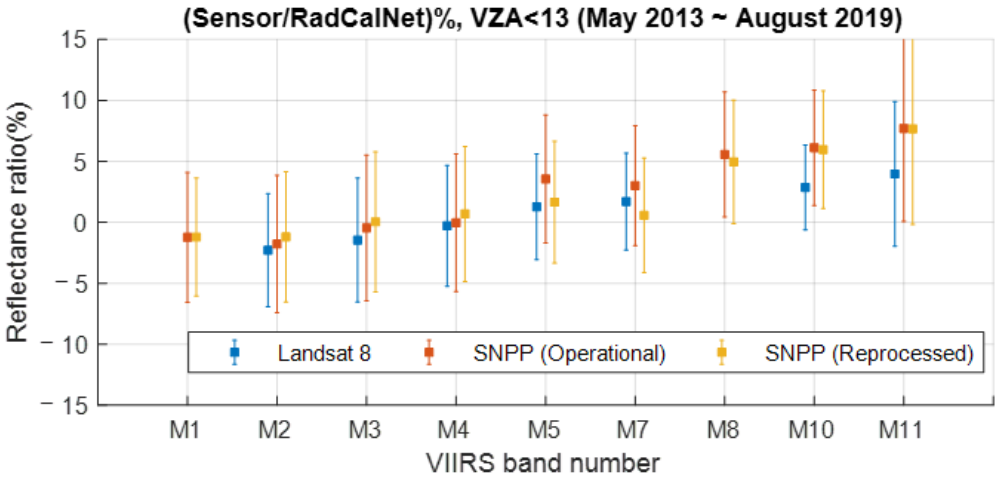

Figure 5. The average reflectance ratio percentage between RadCalNet with Landsat 8/OLI, and operational and reprocessed SNPP/VIIRS at RVUS from May 2013 to August 2019.

Table 3. The mean and standard deviation of the reflectance ratio percentage between RadCalNet with Landsat 8/OLI, and operational and reprocessed SNPP/VIIRS at RVUS from May 2013 to August 2019.

	Sensor vs. RVUS (Bias% ± Standard Deviation%)		
	Landsat 8/OLI	**SNPP/VIIRS Operational**	**SNPP/VIIRS Reprocess**
M1	N/A	−1.23 ± 5.32	−1.20 ± 4.83
M2/B1	−2.29 ± 4.63	−1.77 ± 5.63	−1.19 ± 5.34
M3/B2	−1.45 ± 5.08	−0.46 ± 5.98	0.05 ± 5.74
M4/B3	−0.28 ± 4.95	−0.03 ± 5.64	0.69 ± 5.54
M5/B4	1.28 ± 4.35	3.56 ± 5.25	1.66 ± 5.00
M7/B5	1.71 ± 3.97	3.02 ± 4.92	0.58 ± 4.71
M8	N/A	5.57 ± 5.12	4.96 ± 5.07
M10/B6	2.86 ± 3.48	6.12 ± 4.73	5.97 ± 4.83
M11/B7	3.97 ± 5.93	7.70 ± 7.62	7.68 ± 7.84

The differences in operational and reprocessed VIIRS biases were within 0.72% for all bands, except the M5 and M7 bands, which exhibited bias differences reaching ~2%. This is because the calibration of the operational VIIRS radiometric bands M5 and M7 was overestimated by ~2%, and scaling factors were used in the reprocessed data to correct the issue [1]. Figure 5 shows that the M5 and M7 biases reduced significantly, indicating that the scaling factors efficiently corrected the overestimated calibration issue. Furthermore, the differences between the operational and reprocessed SNPP/VIIRS results were consistent with the results reported in previous work [1].

Furthermore, in order to reduce the comparison uncertainty resulting from the RVUS site, which included variability in the site surface, uncertainty in the ground truth data, Landsat 8/OLI was used as another benchmark with which to evaluate the radiometric performance of VIIRS datasets. To illustrate the differences more clearly in operational and reprocessed VIIRS biases from Landsat 8/OLI, Figure 6 shows the double difference in the average reflectance ratio percentage between SNPP/VIIRS operational and reprocessed data and Landsat 8/OLI via RadCalNet at RVUS from May 2013 to August 2019, and Table 4 lists the results. The most notable phenomenon is that the biases between VIIRS and OLI for bands M5 and M7 reduced by ~2% after being reprocessed, which is consistent with the comparison results of the sensors and RVUS. Moreover, after reprocessing, the biases between VIIRS and OLI for M5 and M7 were closer to 0, again indicating the efficiency of the reprocessing method of the SNPP/VIIRS dataset. For the M2 to M4 bands, both the operational and reprocessed VIIRS biases versus OLI were within 2%, which meets the VIIRS radiometric performance specifications. For M5 and M7, the biases were within 2% after being reprocessed. For the M10 and M11 bands, on the other hand, the biases remained larger than 2%, as can be seen in Figures 5 and 6. In addition to the possible lower solar radiation signal, the reason for the larger bias in the long wavelength (>1200 nm) band could be due to the narrower spectral width of VIIRS as compared with OLI, which results in less radiative energy being detected.

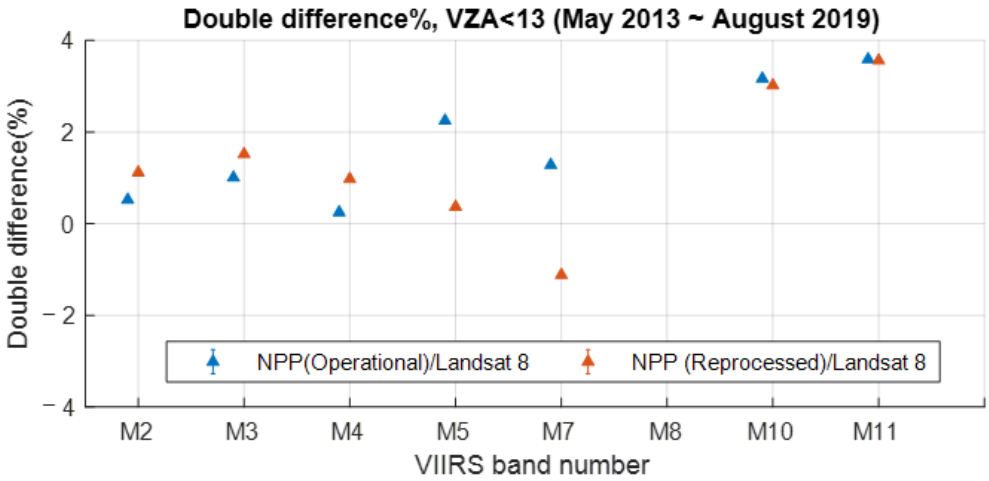

Figure 6. The double difference in the reflectance ratio percentage between SNPP/VIIRS operational and reprocessed data and Landsat 8/OLI via RadCalNet at RVUS from May 2013 to August 2019.

4.1.2. Comparison Results of Yearly Drift

As a result of the continuous data collection by RVUS since May 2013, it is possible to analyze the radiometric stability of the time series in this work over RVUS through the ground truth. Figure 7 shows the time series of the reflectance ratio between Landsat-8/OLI (blue), operational SNPP/VIIRS (red), reprocessed SNPP/VIIRS (green), and RadCalNet over RVUS from May 2013 to August 2019. Overall, the different data records agree well with each other despite certain discrepancies. Furthermore, the obvious shift between the operational and reprocessed VIIRS of M5 and M7 bands can be seen due to the scaling factor correction. In addition, more dispersion of the VIIRS M11 band can be noticed and

may result from the reduced solar radiation signal, the longer wavelength of the detectors, and the narrower spectral width of VIIRS as compared to OLI, which result in less radiative energy being detected, as mentioned above.

Table 4. The mean and standard deviation of the reflectance ratio percentage between Landsat 8/OLI with operational and reprocessed SNPP/VIIRS at RVUS from May 2013 to August 2019.

	SNPP VS. Landsat 8 (Bias%)	
	SNPP/VIIRS Operational-L8	**SNPP/VIIRS Reprocess-L8**
M1	N/A	N/A
M2/B1	0.52	1.10
M3/B2	0.99	1.50
M4/B3	0.25	0.97
M5/B4	2.28	0.38
M7/B5	1.31	−1.13
M8	N/A	N/A
M10/B6	3.26	3.11
M11/B7	3.73	3.71

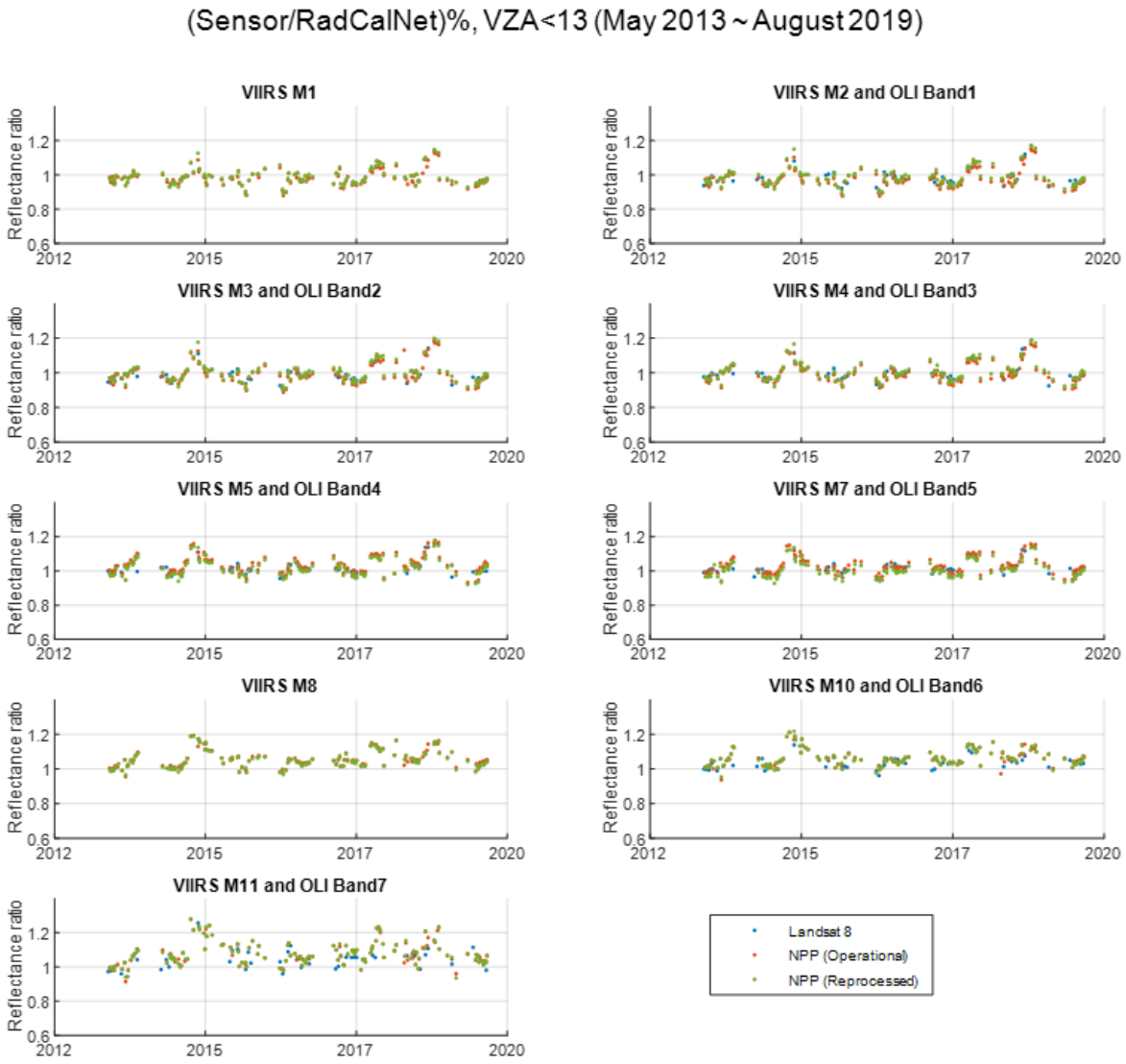

Figure 7. The time series of the reflectance ratio between RadCalNet with Landsat-8/OLI, operational SNPP/VIIRS, and reprocessed SNPP/VIIRS over RVUS from May 2013 to August 2019.

Figure 8 shows the yearly drift and the 95% confidence interval of the reflectance ratio between Landsat 8/OLI (blue), operational (red), and reprocessed (orange) SNPP/VIIRS and RadCalNet at RVUS from May 2013 to August 2019. Table 5 lists the results and the drift differences between operational and reprocessed SNPP/VIIIRS and OLI. It can be seen that all bands of the three datasets exhibited upward trends at the RVUS site. The yearly drift of OLI, operational, and reprocessed VIIRS reached 0.36%/year, 0.60%/year, and 0.45%/year, respectively. However, as can be seen in Figure 8, the consistency of the trends across sensors and datasets suggests that the upward trends were most likely due to a slight degradation of the site. Therefore, here we focus on the yearly drift of the VIIRS datasets as compared with the OLI.

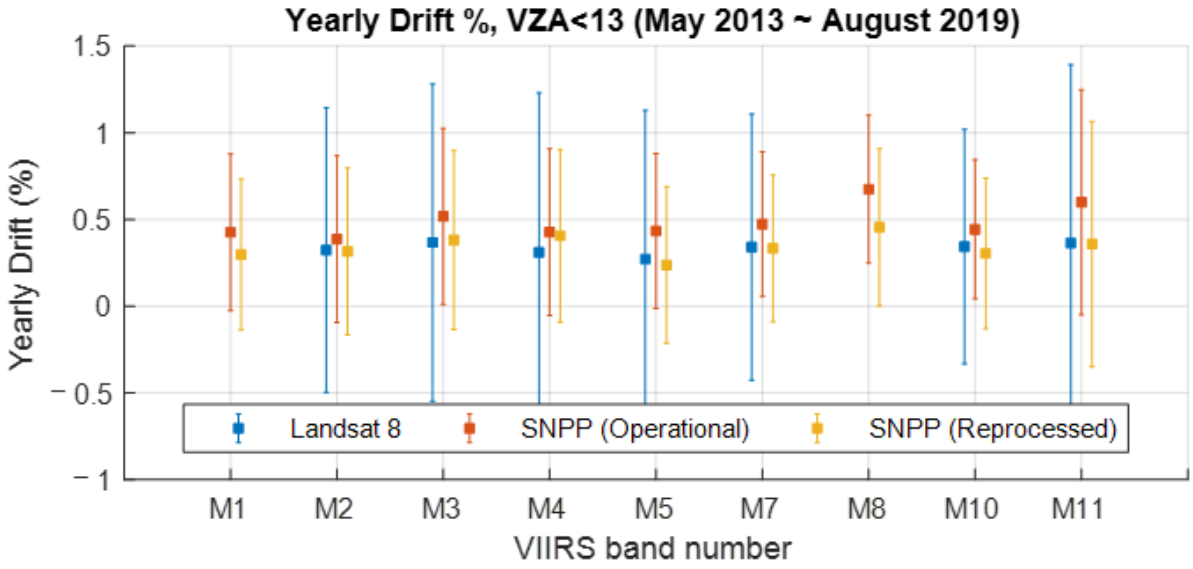

Figure 8. The yearly drift and its 95% confidence interval of the reflectance ratio between RadCalNet with Landsat 8/OLI (blue), operational (red), and reprocessed (orange) SNPP/VIIRS at RVUS from May 2013 to August 2019.

Table 5. The yearly drift and its 95% confidence interval of the reflectance ratio between RadCalNet with Landsat 8/OLI, operational, and reprocessed SNPP/VIIRS at RVUS from May 2013 to August 2019, and the drift difference between operational and reprocessed SNPP/VIIIRS and OLI.

	Yearly Drift% ± 95% Confidence Interval			**Yearly Drift Difference%**	
	Landsat 8/OLI	**SNPP/VIIRS Operational**	**SNPP/VIIRS Reprocess**	**SNPP/VIIRS Operational-OLI**	**SNPP/VIIRS Reprocess-OLI**
M1	N/A	0.43 ± 0.45	0.30 ± 0.43	N/A	N/A
M2	0.32 ± 0.82	0.39 ± 0.48	0.32 ± 0.48	0.07	0.00
M3	0.37 ± 0.91	0.52 ± 0.51	0.38 ± 0.52	0.15	0.01
M4	0.31 ± 0.92	0.43 ± 0.48	0.41 ± 0.50	0.12	0.10
M5	0.27 ± 0.86	0.43 ± 0.45	0.24 ± 0.45	0.16	−0.03
M7	0.34 ± 0.77	0.47 ± 0.42	0.33 ± 0.42	0.13	−0.01
M8	N/A	0.67 ± 0.43	0.45 ± 0.45	N/A	N/A
M10	0.34 ± 0.68	0.44 ± 0.40	0.30 ± 0.43	0.10	−0.04
M11	0.36 ± 1.03	0.60 ± 0.65	0.36 ± 0.71	0.24	0.00

For the equivalent bands, the drift difference between OLI and operational VIIRS was no larger than 0.24%/year, as can be seen in Table 5. On the other hand, the drift difference in the reprocessed dataset between OLI and VIIRS decreased, which was no larger than 0.1%/year, indicating that, after reprocessing, the SNPP/VIIRS reflective bands meet the long-term stability requirement, and are well within the specification of 0.3%/year. Moreover, bands M2, M3, M5, M7, M10, and M11 were shown to be stable to well within

0.04%. This indicates that the reprocessing algorithm efficiently increased the stability of the SNPP/VIIRS dataset and can better serve the broader user community, including the ocean color community, which requires a stringent calibration stability requirement of more than 0.2% [1]. The confidence interval for all bands of the OLI was ~0.4% larger than that of the VIIRS, which is not surprising as OLI has much fewer data points (Table 2).

4.2. SNPP and NOAA-20 Comparison Results

In the previous section, both the RVUS site and Landsat 8/OLI were used as references for evaluating the radiometric performance of operational and reprocessed SNPP/VIIRS VNIR band measurements. It was concluded that after reprocessing, both the radiometric performance and stability of SNPP/VIIRS met the specifications. Alternatively, NOAA-20/VIIRS radiometric performance can be assessed by intercomparing it with SNPP through RVUS using the double difference method, although Simultaneous Nadir Overpass (SNO) does not exist between NOAA-20 and SNPP. Note that, considering the effective time period on the RVUS site in this work and the data release time of NOAA-20, the time period for the evaluation of NOAA-20 was from February 2018 to August 2019. Since only one and a half years of data were used, the temporal stability was not evaluated herein: the main focus was on the evaluation of the radiometric performance of NOAA-20.

Figure 9 shows the average reflectance ratio percentage between reprocessed SNPP/VIIRS (blue), NOAA-20/VIIRS (red), and RadCalNet at RVUS from February 2018 to August 2019. Table 6 lists the results and their double difference results. It can be seen that the reflectance ratio percentage difference between the operational SNPP/VIIRS and NOAA-20/VIIRS was 3–4%, and the difference between the reprocessed SNPP and NOAA-20 reduced to 2–3%, which is consistent with previous evaluations [1,29–31]. In particular, as a result of the scaling factor correction of the SNPP/VIIRS M5 and M7 bands, the differences of the M5 and M7 bands between reprocessed SNPP and NOAA-20 reduced significantly by ~2%.

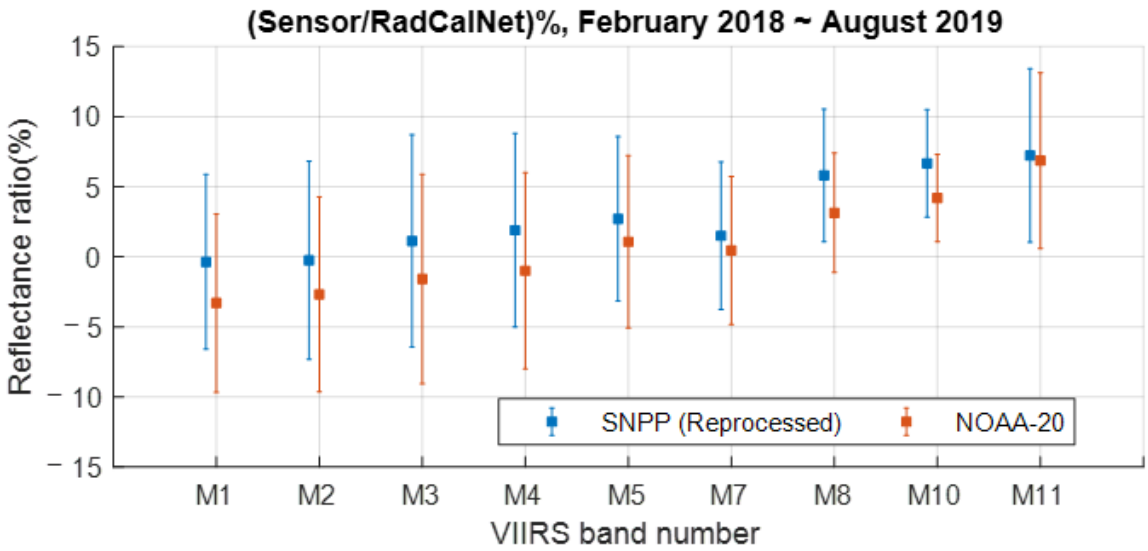

Figure 9. The average reflectance ratio percentage between RadCalNet with reprocessed SNPP/VIIRS and NOAA-20/VIIRS at RVUS from February 2018 to August 2019.

The root cause study for the consistent bias between NOAA-20 and SNPP VIIRS for all RSBs was performed by Moyer et al. (2021) [32]. The study concludes that the uncertainty in the SNPP Solar Diffuser (SD) BRDF characterization during the prelaunch is the most likely cause of bias. In addition, the paper states that, a small part of the bias could also be contributed to by the uncertainty in the sun attenuation screen (SAS) characterization. The study analyzed clocking sensitivity measurements for NOAA-20, J2, and J3 VIIRS. SNPP VIIRS was excluded due to the absence of hardware. The study concluded that clocking could have a significant bias error that should be included in the SD BRDF uncertainty

budget, providing strong evidence that the clocking error in the SD BRDF characterization from S-NPP VIIRS is the likely cause of the VIIRS sensor-to-sensor bias. In future, the intercomparison of SNPP and NOAA-20 VIIRS with J2 VIIRS (planned to be launched in late 2022), can further provide the valuable information on the radiometric accuracy and biases. In addition, the intercomparison with Clarreo Pathfinder (radiometric uncertainty to within 0.3%), planned to be launched in 2023, could eventually help to further understand and confirm the radiometric accuracy of each VIIRS sensors and the source of bias.

Table 6. The mean and standard deviation of the reflectance ratio percentage between reprocessed SNPP/VIIRS, NOAA-20/VIIRS, and RadCalNet at RVUS from February 2018 to August 2019, and their double difference results.

	Reflectance Ratio% ± Standard Deviation%		**Reflectance Ratio%**
	SNPP/VIIRS Reprocess	**NOAA-20/VIIRS**	**Double Difference Reprocessed SNPP-NOAA-20**
M1	-0.36 ± 6.24	-3.30 ± 6.37	2.94
M2	-0.24 ± 7.07	-2.68 ± 6.96	2.44
M3	1.13 ± 7.58	-1.58 ± 7.46	2.71
M4	1.90 ± 6.92	-0.99 ± 7.00	2.89
M5	2.71 ± 5.87	1.08 ± 6.15	1.63
M7	1.50 ± 5.28	0.45 ± 5.29	1.05
M8	5.81 ± 4.73	3.14 ± 4.25	2.67
M10	6.67 ± 3.83	4.20 ± 3.12	2.47
M11	7.23 ± 6.19	6.87 ± 6.27	0.36

5. Conclusions

The two VIIRS sensors onboard the SNPP and NOAA-20 satellites provide high-quality data for critical environmental applications. Thus, it is important to continuously monitor and validate their radiometric performance and stability on orbit. In addition, during the early years of SNPP VIIRS operational calibration and data production, there were inconsistencies in the calibration for a number of reasons. These made time series analyses challenging. Therefore, the NOAA/NESDIS/Center for Satellite Applications and Research developed a comprehensive algorithm, and recalibrated and reprocessed the SNPP/VIIRS radiometric data produced since the launch. This work aimed to validate the radiometric accuracy and stability of the operational and reprocessed SNPP/VIIRS data and the accuracy of the NOAA-20/VIIRS data using the RVUS data from RadCalNet as a benchmark. Since a slight self-degradation was noticed from the RVUS site, Landsat 8/OLI was used as another benchmark for the validation. In addition, given the possible degradation of the RVUS site and given the possible degradation of the RVUS site and the short time period of the NOAA-20 VIIRS data, we solely focused on a stability comparison for the OLI and SNPP VIIRS data. As compared with RVUS and OLI, the radiometric agreement of the operational and reprocessed SNPP/VIIRS bands were within 4% and 2%, respectively, except for the longer wavelength bands, i.e., M8, M10, and M11. The biases of the M5 and M7 bands were reduced by ~2% after reprocessing the SNPP/VIIRS dataset by applying constant scaling over the entire mission. The possible reasons for the larger biases for the longer wavelength bands are the lower levels of solar radiation, and the narrower spectral width of VIIRS as compared with those of OLI. Compared to OLI, the drifts of the operational and reprocessed SNPP/VIIRS data were within 0.24%/year and 0.1%/year, respectively. After reprocessing, the radiometric accuracy and stability of the SNPP/VIIRS data improved and met the SNPP/VIIRS specifications to a good degree. NOAA-20/VIIRS indicated consistently lower responsivity as compared with SNPP, i.e., by ~2 to ~4% for all bands of interest, which is consistent with previous studies.

Author Contributions: Conceptualization, X.J., S.U., T.-C.L., B.Z. and X.S.; methodology, X.J., S.U. and X.S.; software: X.J., T.-C.L. and B.Z.; validation, X.J., S.U. and X.S.; formal Analysis, X.J., S.U. and X.S.; investigation, X.J., S.U. and X.S.; resources, X.J., B.Z. and X.S.; data curation, X.J., T.-C.L., B.Z. and X.S.; writing: X.J., S.U. and X.S.; original draft preparation, X.J.; review and editing, S.U. and X.S.; visualization, X.J. and T.-C.L.; supervision, X.S.; project administration, X.S.; funding acquisition, X.S. All authors have read and agreed to the published version of the manuscript.

Funding: This study was supported by NOAA grant NA19NES4320002 (Cooperative Institute for Satellite Earth System Studies—CISESS) at the University of Maryland/ESSIC.

Acknowledgments: The authors gratefully acknowledge the contribution of the Radiometric Calibration Network (RadCalNet, https://www.radcalnet.org/, accessed on 12 June 2022) and in particular from site Railroad Playa, Nevada, USA (RVUS).

Conflicts of Interest: The authors declare no conflict of interest.

References

1. Cao, C.; Zhang, B.; Shao, X.; Wang, W.; Uprety, S.; Choi, T.; Blonski, S.; Gu, Y.; Bai, Y.; Lin, L.; et al. Mission-Long Recalibrated Science Quality Suomi NPP VIIRS Radiometric Dataset Using Advanced Algorithms for Time Series Studies. *Remote Sens.* **2021**, *13*, 1075. [CrossRef]
2. Jing, X.; Leigh, L.; Pinto, C.T.; Helder, D. Evaluation of RadCalNet Output Data Using Landsat 7, Landsat 8, Sentinel 2A, and Sentinel 2B Sensors. *Remote Sens.* **2019**, *11*, 541. [CrossRef]
3. Bouvet, M.; Thome, K.; Berthelot, B.; Bialek, A.; Czapla-Myers, J.; Fox, N.P.; Woolliams, E.R. RadCalNet: A radiometric calibration network for Earth observing imagers operating in the visible to shortwave infrared spectral range. *Remote Sens.* **2019**, *11*, 2401. [CrossRef]
4. RadCalNet Technical Working Group. *RadCalNet Guidance: Instrumentation and Data Processing (QA4EO-WGCV-RadCalNet-G3_v1)*; Committee on Earth Observation Satellites. 2018. Available online: https://www.radcalnet.org/documentation/RadCalNetGenDoc/G3-RadCalNetGuidance-InstrumentationAndDataProcessing_V1.pdf (accessed on 5 March 2022).
5. Czapla-Myers, J.S.; Thome, K.J.; Leisso, N.P. Radiometric calibration of earth-observing sensors using an automated test site at Railroad Valley, Nevada. *Can. J. Remote Sens.* **2010**, *36*, 474–487. [CrossRef]
6. University of Arizona. *RadCalNet Site Description (QA4EO-WGCV-IVO-CSP-002_RVUS)*; Committee on Earth Observation Satellites: Railroad Valley, NV, USA, 2016.
7. Czapla-Myers, J.; Thome, K.; Wenny, B.; Anderson, N. Railroad Valley Radiometric Calibration Test Site (RadCaTS) as Part of a Global Radiometric Calibration Network (RadCalNet). In Proceedings of the 2020 IEEE International Geoscience and Remote Sensing Symposium, Waikoloa, HI, USA, 26 September–2 October 2020; pp. 6413–6416. [CrossRef]
8. Czapla-Myers, J.; McCorkel, J.; Anderson, N.; Thome, K.; Biggar, S.; Helder, D.; Mishra, N. The ground-based absolute radiometric calibration of Landsat 8 OLI. *Remote Sens.* **2015**, *7*, 600–626. [CrossRef]
9. Reuter, D.; Richardson, C.; Irons, J.; Allen, R.; Anderson, M.; Budinoff, J.; Whitehouse, P. The Thermal Infrared Sensor on the Landsat Data Continuity Mission. In Proceedings of the 2010 IEEE International Geoscience and Remote Sensing Symposium, Honolulu, HI, USA, 25–30 July 2010; pp. 754–757.
10. Markham, B.L.; Barsi, J.A. Landsat-8 Operational Land Imager On-Orbit Radiometric Calibration. In Proceedings of the 2017 IEEE International Geoscience and Remote Sensing Symposium (IGARSS), Fort Worth, TX, USA, 23–28 July 2017; pp. 4205–4207. [CrossRef]
11. USGS. 2017. Available online: https://www.usgs.gov/landsat-missions/landsat-8-oli-and-tirs-calibration-notices (accessed on 19 July 2022).
12. Micijevic, E.; Haque, O.; Mishra, N. Radiometric calibration updates to the Landsat collection. In Proceedings of the In Earth Observing Systems XXI, San Diego, CA, USA, 28 August–1 September 2016. [CrossRef]
13. USGS. Retrieved March 10. 2022. Available online: https://www.usgs.gov/landsat-missions/may-10-2017-landsat-4-8-collection-1-processing-complete (accessed on 12 June 2022).
14. Gascon, F.; Bouzinac, C.; Thépaut, O.; Jung, M.; Francesconi, B.; Louis, J.; Lonjou, V.; Lafrance, B.; Massera, S.; Gaudel-Vacaresse, A.; et al. Copernicus Sentinel-2A Calibration and Products Validation Status. *Remote Sens.* **2017**, *9*, 584. [CrossRef]
15. Markham, B.; Barsi, J.; Kvaran, G.; Ong, L.; Kaita, E.; Biggar, S.; Czapla-Myers, J.; Mishra, N.; Helder, D. Landsat-8 Operational Land Imager Radiometric Calibration and Stability. *Remote Sens.* **2014**, *6*, 12275–12308. [CrossRef]
16. Zanter, K. Landsat 8 (L8) Data Users Handbook. Landsat Science Official Website. 2019. Available online: https://d9-wret.s3.us-west-2.amazonaws.com/assets/palladium/production/s3fs-public/atoms/files/LSDS-1574_L8_Data_Users_Handbook-v5.0.pdf (accessed on 19 July 2022).
17. Uprety, S.; Cao, C. Suomi NPP VIIRS reflective solar band on-orbit radiometric stability and accuracy assessment using desert and Antarctica Dome C sites. *Remote Sens. Environ.* **2015**, *166*, 106–115. [CrossRef]

18. Uprety, S.; Cao, C.; Xiong, X.; Blonski, S.; Wu, A.; Shao, X. Radiometric Intercomparison between Suomi-NPP VIIRS and Aqua MODIS Reflective Solar Bands Using Simultaneous Nadir Overpass in the Low Latitudes. *J. Atmos. Ocean. Technol.* **2013**, *30*, 2720–2736. [CrossRef]
19. Cao, C.; Xiong, J.; Blonski, S.; Liu, Q.; Uprety, S.; Shao, X.; Bai, Y.; Weng, F. Suomi NPP VIIRS sensor data record verification, validation, and long-term performance monitoring. *J. Geophys. Res. Atmos.* **2013**, *118*, 11664–11678. [CrossRef]
20. Gao, C.; Zhao, Y.; Li, C.; Ma, L.; Wang, N.; Qian, Y.; Ren, L. An Investigation of a Novel Cross-Calibration Method of FY-3C/VIRR against NPP/VIIRS in the Dunhuang Test Site. *Remote Sens.* **2016**, *8*, 77. [CrossRef]
21. Mu, Q.; Xiong, X.; Chang, T.; Wu, A. Exploring the stability and residual response versus scan angle effects in SNPP VIIRS sensor data record reflectance products using deep convective clouds. *J. Appl. Remote Sens.* **2018**, *12*, 034006. [CrossRef]
22. Chang, T.; Xiong, X.; Mu, Q. VIIRS Reflective Solar Band Radiometric and Stability Evaluation Using Deep Convective Clouds. *IEEE Trans. Geosci. Remote Sens.* **2016**, *54*, 7009–7017. [CrossRef]
23. Bhatt, R.; Doelling, D.; Coddington, O.; Scarino, B.; Gopalan, A.; Haney, C. Quantifying the Impact of Solar Spectra on the Inter-Calibration of Satellite Instruments. *Remote Sens.* **2021**, *13*, 1438. [CrossRef]
24. Zou, C.-Z.; Zhou, L.; Lin, L.; Sun, N.; Chen, Y.; Flynn, L.E.; Zhang, B.; Cao, C.; Iturbide-Sanchez, F.; Beck, T.; et al. The Reprocessed Suomi NPP Satellite Observations. *Remote Sens.* **2020**, *12*, 2891. [CrossRef]
25. RadCalNet Technical Working Group. RadCalNet Data Format Specification (QA4EO-WGCV-RadCalNet-R2). Committee on Earth Observation Satellites, 26 November. 2019. Available online: https://www.radcalnet.org/documentation/RadCalNetGenDoc/R2-RadCalNetRequirements-DataFormatSpecification_V10.pdf (accessed on 12 June 2022).
26. Jing, X.; Leigh, L.; Helder, D.; Pinto, C.T.; Aaron, D. Lifetime Absolute Calibration of the EO-1 Hyperion Sensor and its Validation. *IEEE Trans. Geosci. Remote Sens.* **2019**, *57*, 9466–9475. [CrossRef]
27. Kaewmanee, M. Pseudo invariant calibration sites: PICS evolution. In Proceedings of the CALCON 2018, Logan, UT, USA, 18–20 June 2018.
28. Uprety, S.; Cao, C. Radiometric performance assessment of Suomi NPP VIIRS SWIR Band (2.25 μm). *Earth Obs. Syst.* **2015**, *9607*, 96072C. [CrossRef]
29. Uprety, S.; Cao, C.; Blonski, S.; Shao, X. Evaluating NOAA-20 and S-NPP VIIRS Radiometric Consistency. In *Earth Observing Missions and Sensors: Development, Implementation, and Characterization V*; International Society for Optics and Photonics: Bellingham, WA, USA, 2018; p. 107810V.
30. Jing, X.; Liu, T.-C.; Shao, X.; Uprtey, S.; Zhang, B.; Sharma, A.S. Validation of GOES-16 ABI VNIR channel radiometric performance with NPP and NOAA-20 VIIRS over the Sonoran Desert. *J. Appl. Remote Sens.* **2020**, *14*, 044517. [CrossRef]
31. Wu, A.; Chang, T.; Xiong, X.; Cao, C. Initial Assessment of Radiometric Performance of N20 VIIRS Reflective Solar Bands Using Vicarious Approaches. In *Earth Observing Missions and Sensors: Development, Implementation, and Characterization V*; SPIE: Bellingham, WA, USA, 2018; pp. 142–153.
32. Moyer, D.I.; Uprety, S.; Wang, W.; Cao, C.; Guch, I. S-NPP/NOAA-20 VIIRS reflective solar bands on-orbit calibration bias investigation. *Int. Soc. Opt. Eng.* **2021**, *11829*, 1182912. [CrossRef]